Progress In Electromagnetics Research B, Vol. 48, 175–196, 2013

ELECTROMAGNETIC SHIELDING FEATURES IN LIGHTWEIGHT PVDF-ALUMINUM BASED NANOCOMPOSITES

Javier Arranz-Andrés[1, *], Nuria Pulido-González[1], Pilar Marín[2, 3], Ana M. Aragón[2, 3], and María. L. Cerrada[1]

[1]Instituto de Ciencia y Tecnología de Polímeros (ICTP-CSIC), Juan de la Cierva 3, Madrid 28006, Spain

[2]Instituto de Magnetismo Aplicado (UCM-ADIF-CSIC), P. O. Box 155, Las Rozas, Madrid 28230, Spain

[3]Departamento de Física de Materiales (UCM), P. O. Box 155, Las Rozas, Madrid 28230, Spain

Abstract—Dependence of the electromagnetic shielding effectiveness on filler volume fraction has been investigated from attenuation upon reflection measurements over a broad frequency range in hybrids based on Poly(vinylidene fluoride)-Aluminum nanoparticles. The loss of reflectivity with relation to the incident radiation in these nanocomposites compared with the pristine polymeric matrix shows the maximum value for the sample with an aluminum content of 10% in volume. Furthermore, the morphological aspects of all the specimens as well as their thermal properties, viscoelastic behavior and dielectric response have been evaluated. The nanocomposite that incorporates an Al content of 10% in volume exhibits the best balance in properties including, in addition to its shielding behavior, its processability and mechanical performance.

1. INTRODUCTION

Electromagnetic interference (EMI) is considered a modern environmental pollution because of the development of sophisticated electronic devices for industrial, commercial, and military applications, whose performance is affected by the electric and electronic signals emitted by other equipments. Accordingly, electromagnetic radiation absorbing materials have been the focus of much research due to increasing

Received 11 December 2012, Accepted 25 January 2013, Scheduled 26 January 2013

* Corresponding author: Javier Arranz-Andrés (jarranz@ictp.csic.es).

government regulation to control levels of electromagnetic radiation, and also to new norms and standards issued regarding compatibility and electromagnetic interference produced by this type of devices [1]. These materials are also important tools in electronic warfare, since they can be used to camouflage potential targets from radar detection.

Electromagnetic radiation absorbing materials have dielectric and/or magnetic losses, and the dependence of these losses on frequency is responsible for their performance, resulting in the absorption and/or scattering of electromagnetic waves. Metals are particularly suitable as shielding material against electromagnetic fields due to their high electrical conductivity (order of magnitude 10^6 Siemens/cm) [2]. Depending on the electromagnetic properties, the material can be either used as an absorber or a reflector of electromagnetic radiation [3, 4]. However, there are few drawbacks when metal is used as a shielding material, its weight as well as its easiness to corrosion being the most important ones.

Polymer–matrix composites containing conductive fillers are attractive for shielding [5] due to their processability (e.g., moldability), which helps to reduce or eliminate the seams in the housing that is the shield. The seams are commonly encountered in the case of metal sheets as the shield and they tend to cause leakage of the radiation and diminish the effectiveness of the shield [6, 7]. In addition, polymer–matrix composites are attractive because of their low density. The polymer matrix is commonly electrically insulating and does not contribute to shielding, though the polymer matrix can affect the connectivity of the conductive filler and connectivity enhances the shielding effectiveness. This effectiveness has been proved in composites based on cooper microwires for microwave attenuation [8]. Magnetic microwires have also shown interesting properties as electromagnetic radar absorbing materials [9, 10]. Furthermore, electrically conducting polymers [11] are becoming increasingly available, but they are not commonly used because of their poor processability and deficient mechanical properties. A great deal of research has been conducted on the use of polymeric composites for EMI shielding applications. For instance, carbon-black and carbon-fiber filled ethylene-vinyl acetate copolymer and natural rubber were prepared [12], studying their potential applications for EMI shielding in both the microwave (100–2000 MHz) and X-band region (8–12 GHz). Similarly, composite materials made from silicone rubber with carbon powder and ferrite powder have been studied in microwaves and terahertz frequency ranges [13]. Several investigations were carried out for the estimation of shielding effectiveness and reflectivity of layered laminate structure made for combination of different materials. In this way, polymer-based

carbon-filled composites [14], or a sandwich of conductive polymer between a conductor and microwave absorber (i.e., Ca-NiTi hexa ferrite, carbonyl-iron particles, barium ferrites, MnZn ferrite) [15] can be used for wideband microwave shielding structures. Other laminated shields are considered as the combination of several layers constructed using conductive polymer, i.e., polyacetylene and poly-p-phenylene-benzobis-thiazole (PBT), doped with iodine, and conducting materials like copper and aluminum [16]. The protection of a sensitive car-size system against electromagnetic waves have been proposed using a shielding cover composed of a 4 layer stuff, aluminum, polyethylene, aluminum and polyester [17]. If the same level of protection could be achieved with one layer, prepared in a one step process, the method would be cheaper.

Dielectric and conductivity properties of composite systems based on polyvinyl chloride (PVC) and polymethyl methacrylate (PMMA) filled with metal powders of Al and Cu have been studied [18]. Similarly, $BaSrTiO_3$, nanosize silicon, silver and Al_2O_3 additives have been considered in combination with other polymer matrices [19]. An increase of relative permittivity in the composites with the inclusion of nanoparticles is desirable in shielding applications. On this mater, PVDF-Cu nanocomposites have shown an exceptional behavior as shielding materials in the X-ray region [20].

Poly (vinylidene fluoride), PVDF, shows excellent mechanical properties, high continuous use of temperature and strong piezoelectricity. These characteristics made possible various scientific and industrial applications of PVDF, as an ultrasound transducer in non-destructive evaluation and medical ultrasound [21–23] and to prepare conducting composites for self-regulated heaters, current protectors, antistatic shielding and conducting electrodes for lithium batteries. It is, therefore, very promising polymeric matrix in electromagnetic radiation absorbing (nano)composite field. The phase behavior of PVDF has been studied intensively, leading to the most important crystal phases: α (form II), β (I), γ (III), and δ (IV). Extensive literature exists on the conditions under which specific phases are obtained; a discussion without ending, because the crystal phases are close in terms of stability and thus small changes in processing conditions may cause another phase to appear. At present, it is understood that at room temperature, it is the α-phase that forms most readily and close to the melting point it is the γ-phase [24–26]. The β-phase, which has the largest ferroelectric moment, appears to be the stable phase at higher pressures [27, 28], and once obtained it does not normally convert into other phases under ambient conditions. There is an abundance of literature describing the interconversion of one phase into another [24–26].

Key parameters to overcome the weight problem of metals are, in these polymeric based composites, on one hand, the use of a content of metal particles as low as possible and, on the other hand, the choice of metals as light as feasible. Therefore, the aim of the current research is to prepare and comprehensively characterize novel hybrids based on PVDF and aluminum (Al) nanoparticles. Aluminum is selected because of its remarkable low density and for its ability to resist corrosion. The use of Al nanoparticles, instead of those particles with micrometric size, has been done as an attempt of reducing metal content in the ultimate material. For instance, in the case of shielding clothing, stainless metal fibers and cotton fibers are used [29]. The use of aluminum would make this type of materials lighter. Other important aspect to be considered is the skin effect [2, 30]. Because of it, a composite material having conductive fillers with small size is more effective than another one containing conductive fillers with a large unit size.

Several techniques have been then required: an anechoic chamber to evaluate electromagnetic response; broad-band dielectric spectroscopy to examine dielectric behavior; dynamic thermal analysis to study viscoelastic properties; and, thermogravimetry to study thermal stability under inert and air environments.

2. EXPERIMENTAL PART

2.1. Materials

A commercially available poly (vinylidene fluoride), PVDF, with trade name of Kynar 741 (kindly supplied by Arkema), has been used in the present research. Aluminum, Al, nanoparticles (IOLITEC) with an average particle size of 18 nm, have been employed in the present research.

2.2. Nanocomposite and Film Preparation

Hybrids with different contents in Al nanoparticles (1, 2, 5, 8, 10, 15 and 20% in volume), labeled as Al1, Al2, Al5, Al8, Al10, Al15 and Al20, respectively, were prepared through melt processing at 190°C and at 120 rpm for 40 min in a Haake Minilab (Thermo Electron Corporation) twin-screw extruder with a volumetric capacity of 7 cm^3 using corotating conical screws.

After extruding the two components, films with similar thickness were obtained by compression molding in a Collin press between hot plates (210°C) at pressures from 2 to 6 MPa for 5 min. A fast quench (around 80°C/min) between plates of the press refrigerated

with cold water was applied to the different films from the melt to room temperature.

2.3. Characterization and Properties

An anechoic chamber is used to study electromagnetic behavior where two TEM horn antennas (EMCO3160-07) are placed in the far field (Fraunhofer region) of the absorbing material. Their bandwidth goes from 7 to 15 GHz. The absorbing material is placed in front of a metallic plate that ensures total reflection. The plate dimension is $25\times25\,\mathrm{cm}^2$. They are surrounded by the same absorbers of the anechoic chamber to avoid border effects. In our experiments a metallic sheet is covered by a dielectric slab of thickness d_3 and a PVDF-Aluminum based composites of thickness d_2 is located over them covering the assembly. Therefore the electromagnetic radiation is incident on the composite slab, goes through it and the dielectric and is reflected by the metallic surface [11]. The reflection coefficient at the surface of the composite slabs, R_0 [8], depends on air, dielectric and composite impedances and on dielectric and composites thickness d_3 and d_2. Since the TEM horn antennas are in the farfield the waves can be considered planar waves, propagating in TEM mode. The antennas are connected to a Network Analyzer (AgilentE8362BPNA Series Network Analyzer), and S_{12} is measured, after careful calibration procedure based on open air measurements where S_{12} is the reverse transmission coefficient of 50 W terminated input. Both real and imaginary part of R_0 are measured and R is represented and defined from the modulus, $|R_0|$, as

$$R = 20\log(|R_0|)\ (\mathrm{dB})$$

Scanning electron microscopy (SEM) experiments were carried out with a XL30 ESEM PHILIPS equipment. The samples were cryo-fractured prior to SEM observations.

The electrical properties were measured with a Novocontrol BDS system comprising a frequency response analyzer (Solartron Schlumberger FRA 1260) and a broadband dielectric converter with an active sample head. Gold disk electrodes (20 mm in diameter) were used in the dielectric measurements carried out at 25°C in the frequency window 10^{-1} to 10^7 Hz. The temperature was controlled by a nitrogen jet (QUATRO from Novocontrol) with a temperature error of 0.1 K during every single sweep in frequency.

The complex permittivity ε^* of the samples were calculated from the measurement of the complex impedance Z^* given by $Z^* = V^*/I^*$, where V^* and I^* are the voltage and current circulating through the sample at a certain angular frequency ω. Once the impedance has been measured, ε^* can be calculated by means of $\varepsilon^*(\omega) = \varepsilon' - i\varepsilon'' =$

$-i/\omega Z^*(\omega)C_0$, where ε' and ε'' are the real and imaginary part of the complex permittivity and C_0 corresponds to capacity of the empty sample holder. The specific conductivity σ^* is related to the dielectric function by $\sigma^* = \sigma' - i\sigma'' = i2\pi f\varepsilon_0(\varepsilon^* - 1)$ where ε_0 is the vacuum permittivity.

Viscoelastic properties were measured with a Polymer Laboratories MK II dynamic mechanical thermal analyzer working in the tensile mode. The real (E') and imaginary (E'') components of the complex modulus and the loss tangent ($\tan\delta$) of each sample were determined at 1, 3, 10 and 30 Hz, over a temperature interval ranging from −140 to 160°C, at a heating rate of $1.5°C\,min^{-1}$. The apparent activation energy values were estimated on $\tan\delta$ according to an Arrhenius-type equation, employing an accuracy of 1°C in the temperature assignment maxima. The frequency dependence on temperature in the relaxation mechanisms associated to the glass transition has been also considered to follow an Arrhenius behavior though it is due to cooperative motions [31]. This approximation can be made without a significant error, since the range of analyzed frequencies is low enough to be fitted to such a linear behavior just mentioned.

Calorimetric analyses were carried out in a TA Instruments Q100 calorimeter connected to a cooling system and calibrated with different standards. The sample weights ranged from 7 to 10 mg and the heating rate used was $20°C\,min^{-1}$. For crystallinity determinations, a value of $104.5\,J\,g^{-1}$ has been taken as enthalpy of fusion of a perfect crystalline material [20, 32].

The thermal stability measurements of the various samples were carried out by using a TA Q500 thermogravimetric analyzer (TGA) in the temperature range 20–800°C under both air and nitrogen atmospheres.

3. RESULTS AND DISCUSSION

All the PVDF nanocomposites here analyzed exhibit a semicrystalline character, and incorporation of Al nanoparticles does not change the crystalline polymorph developed by the PVDF matrix. Consequently, the majority cell obtained is the α-phase, which is the most stable crystalline form of PVDF when crystallizing from the melt. It crystallizes in a non-polar TGTGN configuration, leading the consecutive permanent dipoles of the monomer units to orient in opposite directions, resulting in no net dipole per unit cell [33]. Nevertheless, some small changes occur within PVDF crystalline regions because of the Al presence, as clearly noticed in Figure 1. Then, melting temperatures increase slightly in composites with low

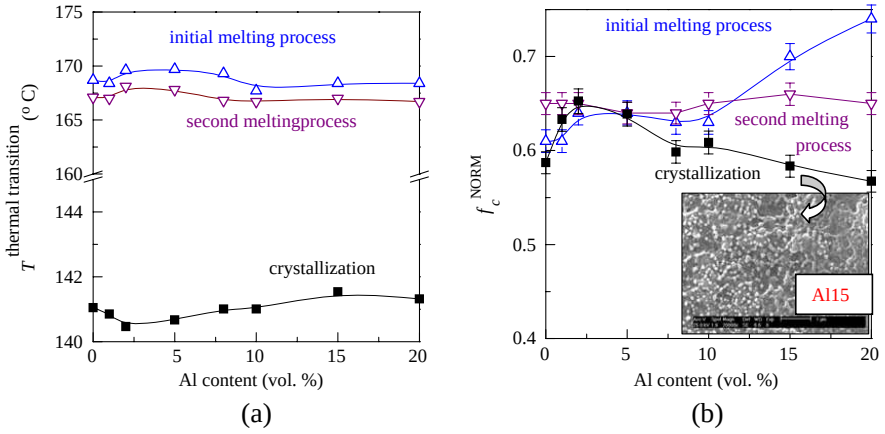

Figure 1. Variation with Al vol.% content of (a) thermal transition temperatures and (b) crystallinity values obtained in the temperature interval ranging from 0 to 180°C for the initial melting, crystallization and second melting processes, respectively. The SEM picture for Al15 composite is attached as inset.

Al contents (see Al2, Al5 and Al8 hybrids) while their crystallization takes place at lower temperatures, as deduced from Figure 1(a). On the other hand, Al nanoparticles act as nucleating agent at high concentration and this transition shifts to slightly higher temperatures. Moreover, PVDF crystallinity is also affected by the Al presence. Then, degree of crystallinity estimated from the initial melting process shows a slight raise at low Al nanoparticle incorporation and a significant increase at Al contents higher than 10 wt.%. The further cooling run from the molten state shows, on the contrary, that those samples with the highest Al concentration now develop lower crystallinity than those with inferior Al content. Crystallinity for all of the samples remains, however, almost unchanged in the subsequent melting process. All these features seem to indicate that high contents of Al nanoparticles provoke a nucleating effect (i.e., crystallization begins at higher temperatures) but slow down the PVDF crystallization process and, then, crystallinity during cooling is considerably reduced at those high Al incorporations. If Al15 and Al20 samples stay at room temperature enough time (as seen from results of initial melting processes) initially amorphous PVDF macrochains are able to be ordered into three-dimensional entities, exhibiting the highest degrees of crystallinity.

SEM micrographs show that Al nanoparticles dispersion and

distribution and, accordingly, homogeneity within the hybrid materials are rather good. Absence of detectable metallic domains of large size across specimens is deduced even at the highest Al contents (see inset in Figure 1(b)). The average size of Al aggregates is ranging from around 40 to 175 nm, fact that indicates that preparation method has been fairly efficient.

3.1. Electromagnetic Characteristics

One of the most attractive aspects of these materials is their EMI shielding behavior. The effectiveness of a shield can be indicated by either the surface resistivity or the volume resistivity. This is because of the fundamentally different ways in which these processes act to reduce EMI. In either case, the measure is an indicator only and the shielding achieved on the final material is the actual measure of the effectiveness of the process. The actual indicator is the shielding effectiveness (SE) achieved in the actual environment (i.e., the attenuation of the electromagnetic field after the shield has been introduced). This is expressed in decibels (dB) by the formula:

$$\mathrm{SE} = 20 \log(\mathrm{EM}_{\mathrm{reflected}}/\mathrm{EM}_{\mathrm{incident}})$$

The actual attenuation for any EMI shielding method is strongly dependent on the frequency of the incident radiation and shielding methods are rarely equally effective across the wide range of electromagnetic radiation frequencies experienced in real life. The methodology used for the current investigation works from 7 to 15 GHz, as aforementioned in the Experimental Section.

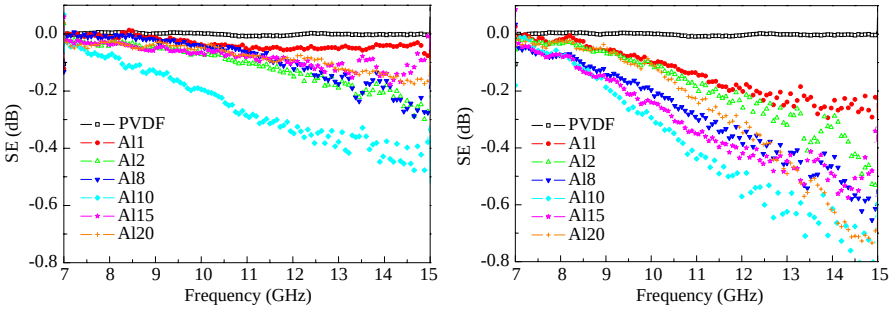

Figure 2. Return loss of the reflection coefficient (R_0) versus frequency of PVDF and different nanocomposites: (a) at a 0 μm; (b) at 1000 μm distance from the metal layer.

Figure 2(a) shows EMI shielding effectiveness (SE) from attenuation upon reflection for the different nanocomposites analyzed placed on a metal layer. It is clearly observed a loss of reflectivity with relation to the incident radiation in the nanocomposites compared with the almost constant response, close to zero, exhibited by the pristine PVDF matrix in the whole frequency range analyzed. This figure also proves that Al10 nanocomposite presents the best shielding behavior. This response should be understood in terms of composite dielectric constant. The lowest Al contents are not sufficient to influence the composite electromagnetic properties and do not allow reaching the maximum reduction while the highest Al compositions in Al15 and Al20 samples are not efficient enough because of presence of more Al aggregates that could turn out in partial reflections.

The effect of distance of the nanocomposite films related to the metal layer has been also checked and Figure 2(b) shows a similar behavior than that just commented, i.e., a loss of reflectivity in the nanocomposites regarding the PVDF polymeric matrix and the Al10 materials as the one with the optimum response. Nevertheless, the shielding effectiveness is now much larger.

The Al10 nanocomposite has been taken to further analyze this effect and its EMI properties have been examined at different distances of the film from the metal layer. In this case, between metal and composite sample, a "glaspack" sheet of width between 0 and 1000 μm, has been placed. Figure 3 represents the reduction in reflectivity that the Al10 nanocomposite undergoes with distance. In order to understand this feature the following considerations should be done. The electromagnetic radiation is incident on the composite slab in the performed experiments, it goes through it and the dielectric "glaspack" and it is reflected by the metallic surface. The reflection coefficient depends on composite impedance and on distance, d, from the composite to the metal and it is minimum when $\varsigma + 2\gamma_1 d = \pi$ where γ_1 is composites wave vector ad ς is given by [8].

$$\varsigma = -2\tan^{-1}\left(\frac{Z_2}{Z_1}\tan\gamma_2 d_2\right)$$

where, Z_1, and Z_2, are the composite and dielectric impedance, respectively, and γ_2 is the dielectric wave vector and d_2 is the distance between dielectric sheet and metal. This rule can be used as a guide for an approximate control of frequency of the maximum attenuation, as a function of composite and dielectric thickness and impedances. At a certain composite impedance (or dielectric constant) the higher the distance is between metal and composite, the lower the frequency is associated with the minimum reflectivity.

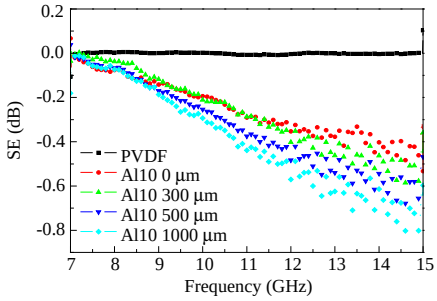

Figure 3. Return loss of the reflection coefficient (R_0) versus frequency of PVDF and Al10 nanocomposite at different distances from the metal layer.

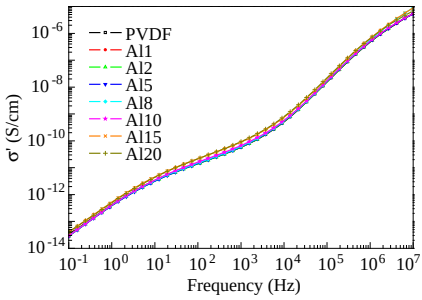

Figure 4. Electrical conductivity measured at 25°C as a function of frequency for PVDF-Al nanocomposites.

The performed experiments have demonstrated this behavior for the composites under study. The attenuation level goes from −0.4 dB to −0.8 dB for 15 GHz because of the composite impedance (see Figure 3).

3.2. Electric Properties

Once the electromagnetic response of these PVDF nanocomposites has been evaluated, the knowledge of their dielectric behavior is of great interest. Therefore, the electrical conductivity, σ, as a function of frequency for the samples with different volume concentration of aluminum is shown in Figure 4 and its value at 100 Hz is listed in Table 1. PVDF and all of the nanocomposite materials exhibit strong frequency dependence, even those that incorporate the highest Al contents, and, accordingly, σ increases with frequency with a slope close to 1. This behavior is characteristic of insulating materials. Consequently, the insulator-conductor transition is not taking place within the Al composition range here analyzed, probably because percolation threshold has not been reached. This response is unlike to that found in PVDF based composites containing Cu nanoparticles as metal component since they became conducting at around 7 vol.% [21]. Differences can be attributed to inherent characteristics between Cu and Al particles, such as their either own conductivity or density. Anyway, it seems to be then deduced from these results that conductivity is not absolutely required for exhibiting a good electromagnetic performance, although this could be even better in conductive materials.

Table 1. Conductivity (σ) and real dielectric permittivity values at 100 Hz and 25°C as well as frequency location (f) and intensity of α_C relaxation on $\tan\delta$ basis.

Sample	σ (100 Hz) $\cdot 10^{11}$ (S/cm)	ε' (100 Hz)	α_C relaxation on $\tan\delta$	
			f (Hz)	intensity $\cdot 10^2$
PVDF	1.4	7.0	2.2	8.9
Al1	1.5	7.2	2.2	8.7
Al2	1.4	7.4	2.2	8.3
Al5	1.4	7.6	2.2	7.9
Al8	1.5	7.6	2.2	8.3
Al10	1.6	8.1	3.4	7.9
Al15	2.1	9.7	3.4	8.5
Al20	2.1	10.3	3.4	7.7

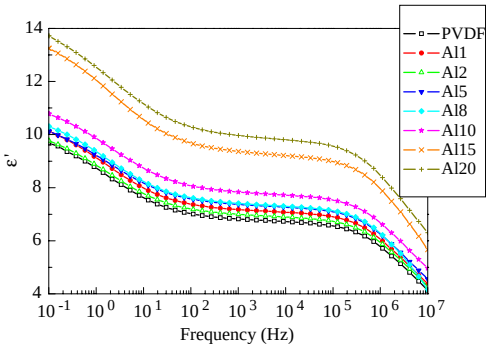

Figure 5. Real dielectric permittivity measured at 25°C as a function of frequency for PVDF-Al nanocomposites.

To investigate the dielectric behavior of these PVDF-Al nanocomposites, dielectric permittivity and tan δ of the samples are obtained at room temperature in the frequency range from 10^{-1} to 10^7 Hz. The variations of the real part of the dielectric permittivity, ε', for the PVDF and the nanocomposites with different Al nanoparticle volume fractions as a function of frequency are presented in Figure 5. In addition, some numerical features are reported in Table 1. An increase in the value of ε' is observed within the whole frequency range analyzed in the hybrid materials when compared with the pristine PVDF matrix, this rise being more significant for those containing the highest Al contents. This feature points out that polarizability

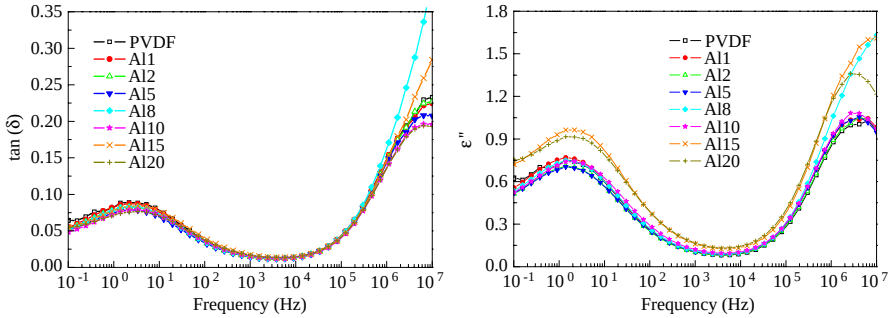

Figure 6. Loss tangent and imaginary dielectric permittivity measured at 25°C as a function of frequency for PVDF-Al nanocomposites.

is raised as Al nanoparticle content becomes higher in the different materials. Furthermore, almost parallel frequency dependence is seen in all of the samples.

The $\tan\delta$, also called loss tangent, dielectric loss or the "dissipation factor" is the ratio of the imaginary to the real part $(\varepsilon''/\varepsilon')$, where δ is called as the "loss angle" and denotes the phase angle between the voltage and the current. Tanδ is, then, another important parameter in dielectric materials, which is caused by conductive loss of motion of charge carrier and/or dipole loss of dipole orientation polarization [34]. The $\tan\delta$ and ε'' curves at room temperature of these samples as a function of frequency are shown in Figure 6. Two relaxation processes are observed in both magnitudes in the frequency ranged studied. The peak located at around 10^6–10^7 Hz is associated with the glass transition process in the PVDF and it is labeled as α relaxation. It is then caused in the PVDF main chains by cooperative micro-Brownian motions within their amorphous regions [35, 36]. The process at about 10^0 Hz is ascribed to the molecular motions within the crystalline fraction of the PVDF material and it is named as α_C relaxation [37–40]. The presence in all the specimens of this relaxation associated with motions within crystallites confirms that the primary polymorph developed is the non-polar α-phase since it practically disappears when β crystals are majority [41].

Figure 6 also shows that dielectric losses are slightly higher along the frequency range measured in the specimens with the largest Al incorporations. As seen in $\tan\delta$ dependence, the location of α_C relaxation peak is shifted slightly toward higher frequencies (shorter times) in the ε'' representation, indicating that the motions involved in this process occur faster. All of these characteristics point out

the feasible applicability of these composites for decoupling capacitor applications [42].

3.3. Viscoelastic Behavior

The knowledge of mechanical performance is other key feature for final applications of these PVDF-Al hybrids. The dynamic mechanical thermal analysis is chosen to evaluate the viscoelastic response in bulk since it allows obtaining rather complete information over a wide temperature range. It provides information on relaxation processes, either those related to the generalized glass transition or those ones associated with local motions, as well as on macromolecular stiffness. Two relaxation mechanisms were observed from the dielectric spectra analyzed at room temperature over a wide frequency range while Figure 7 proves that the pristine PVDF and the different composites exhibit three mechanical relaxation processes under tension in the representations of loss magnitudes at this temperature range examined, labeled as γ, β, and α in order of increasing temperatures [43, 44]. The γ relaxation, located at around $-80°$C, has been attributed to molecular motions that take place in amorphous regions. This mechanism clearly overlaps with the β relaxation that appears around

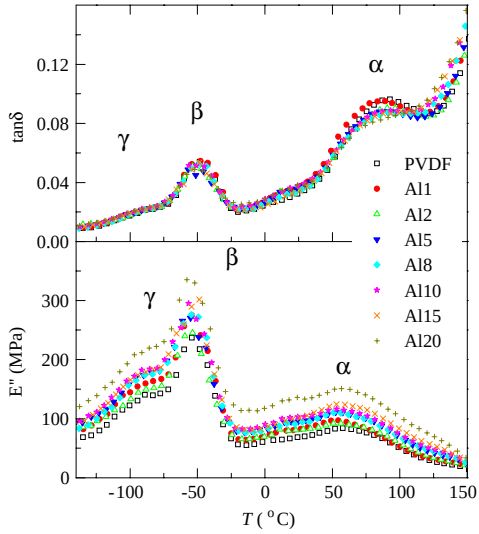

Figure 7. Temperature dependence at 3 Hz of the loss tangent and imaginary component of complex modulus (upper and lower plot, respectively) for PVDF-Al nanocomposites.

Table 2. Relaxation temperatures, apparent activation energies for the main relaxation processes (in $\tan\delta$ basis) found in the different hybrids at 3 Hz as well as storage modulus values at 25°C.

Sample	Al (vol.%)	T (°C)		ΔH (kJ/mol)		E′ 25°C (MPa)
		β	α	β	α	
PVDF	0	−49	92	300	100	2100
Al1	1	−48	87	300	100	2250
Al2	2	−50	94	300	100	2275
Al5	5	−50	91	300	100	2650
Al8	8	−49	94	300	100	2725
Al10	10	−50	92	300	100	2700
Al15	15	−50	93	300	100	2950
Al20	20	-50	95	300	100	3550

−50°C and corresponds to the PVDF glass transition. Location of this primary relaxation process on $\tan\delta$ basis is rather independent of Al nanoparticle incorporation, as deduced from Table 2, although its intensity is slightly reduced, fact that could be associated with differences in the crystallinity degree (see Figure 1) and, then, the lower amorphous content in Al15 and Al20.

The α relaxation, attributed to movements in the crystalline regions, is observed in PVDF and nanocomposites at around 90°C. A reduction of its intensity is again seen with increasing Al concentration in the final materials. Consequently, the mobility restrictions that the presence of Al nanoparticles imposes not only affect the amorphous phase but also the crystalline regions.

Concerning the apparent activation energies, it can be commented that identical energy is involved in each mechanism, the one ascribed to glass transition and that associated with motions in the crystalline regions, independently of the Al content. Incorporation of nanoparticles causes some mobility variations within the polymeric PVDF matrix but these changes are not of great magnitude.

Moreover, storage modulus, E', is obtained from this technique for the different materials analyzed. E' is related to the stiffness of nanocomposites and its variation on temperature at the distinct Al nanoparticle content is depicted in Figure 8. Incorporation of the Al nanoparticles increases significantly the rigidity in the hybrids in the whole temperature interval examined. In addition, E' values at 25°C are represented in the inset. This feature can be attributed in these materials to two different effects: on one hand, the own reinforcement that Al nanoparticles provide to the PVDF matrix; and,

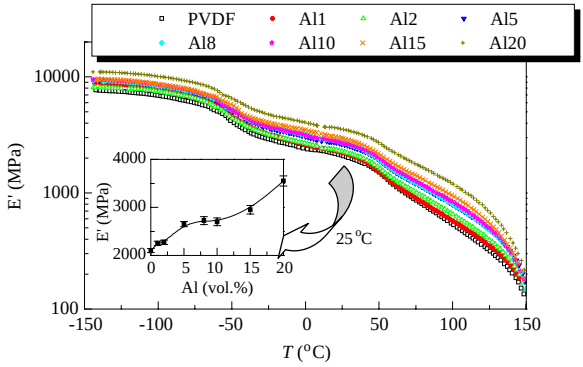

Figure 8. Temperature dependence at 3 Hz of real component of complex modulus for PVDF and its composites with aluminum. In the inset: variation of E' on Al content at 25°C.

on the other hand, the increase in PVDF crystallinity observed as Al content is raised (see Figure 1(b)). This stiffness enlargement has been also observed from stress-strain and microhardness experiments not reported here.

E' values change on Al content more significantly at temperatures higher than around −50°C, due probably to the more prominent effect of the rigid components (Al nanoparticles and PVDF crystallites) on mechanical performance at temperatures above glass transition where PVDF mobility considerably increases.

3.4. Thermal Stability

The PVDF-Al hybrids under study exhibit very interesting electromagnetic characteristics and an appropriate mechanical performance. An additional requirement is to analyze their thermal stability and learn how this feature changes with Al nanoparticle incorporation. Figure 9 displays the TGA results related to the distinct samples under inert and oxidant conditions. Significant differences in the degradation behavior are perceptible depending on the experimental conditions used during experiments. Looking first at curves achieved under a nitrogen atmosphere (left plot in Figure 9), one primary degradation process and another secondary one at higher temperatures are clearly detectable in the neat PVDF. The maximum weight loss of the main decomposition mechanism is located at around 490°C as reported in Table 3. The PVDF degradation processes implies the formation of different species, such as HF, with the destruction of the original polymer structure and the formation of a conjugated system, crosslinking,

Table 3. Characteristic decomposition temperatures under nitrogen and oxidant atmospheres: the temperatures of 5%, $T_{5\%}$, and 10%, $T_{10\%}$, mass loss as well as the temperatures at the maxima, $T_{\max}$. Column W^{800} represents the weight remaining at 800°C.

Sample	Al wt.%	Inert atmosphere				Air atmosphere				
		$T_{5\%}$ (°C)	$T_{10\%}$ (°C)	$T_{\max}$ (°C)	W^{800}	$T_{5\%}$ (°C)	$T_{10\%}$ (°C)	$T_{\max 1}$ (°C)	$T_{\max 2}$ (°C)	W^{800}
PVDF	0.0	463	472	490	19	414	433	471	522	0
Al1	1.5	366	377	392	32	357	367	386	537	2
Al2	3.1	365	376	392	37	355	365	382	536	4
Al5	8.0	361	373	391	42	351	360	376	540	8
Al8	13.2	350	362	387	46	348	357	373	542	14
Al10	16.9	349	360	387	50	348	359	384	537	20
Al15	26.8	352	364	385	58	346	354	372	550	30
Al20	37.9	350	360	381	60	345	354	368	565	40

branching, and polyene formation, increasing degradation at temperatures ranging 400–600°C results in the aromatization and ultimately polyaromatization [45–47].

Incorporation of Al nanoparticles involves a very significant catalytic effect on thermal stability even at a content as low as 1.5 wt.%. Then, an important shift to inferior temperatures is observed for all of the hybrids, around 100°C compared with PVDF matrix (see results summarize in Table 3). Presence of Al nanoparticles triggers degradation although these composites are stable enough for regular applications. The primary decomposition seems to be composed of two overlapped processes and moves slightly to lower temperatures as Al content is further raised. A smaller displacement has been recently reported using multiwalled carbon nanotubes [48] while this behavior is completely dissimilar to that lately described in PVDF-Cu nanocomposites [20], where incorporation of Cu nanoparticles maintained and even slightly improved thermal stability in experiments performed under inert conditions. However, a significant residual amount remains in both cases at temperatures above 600°C, like in the current materials.

On the other hand, two stages are seen in the overall decomposition process under air conditions in all the samples (Figures 9(b) and (d)). It is observed that incorporation of Al nanoparticles reduces thermal stability of the first degradation stage while the second one becomes stabilized (see Table 3) and, therefore, its beginning is postponed. Moreover, neat PVDF does not present

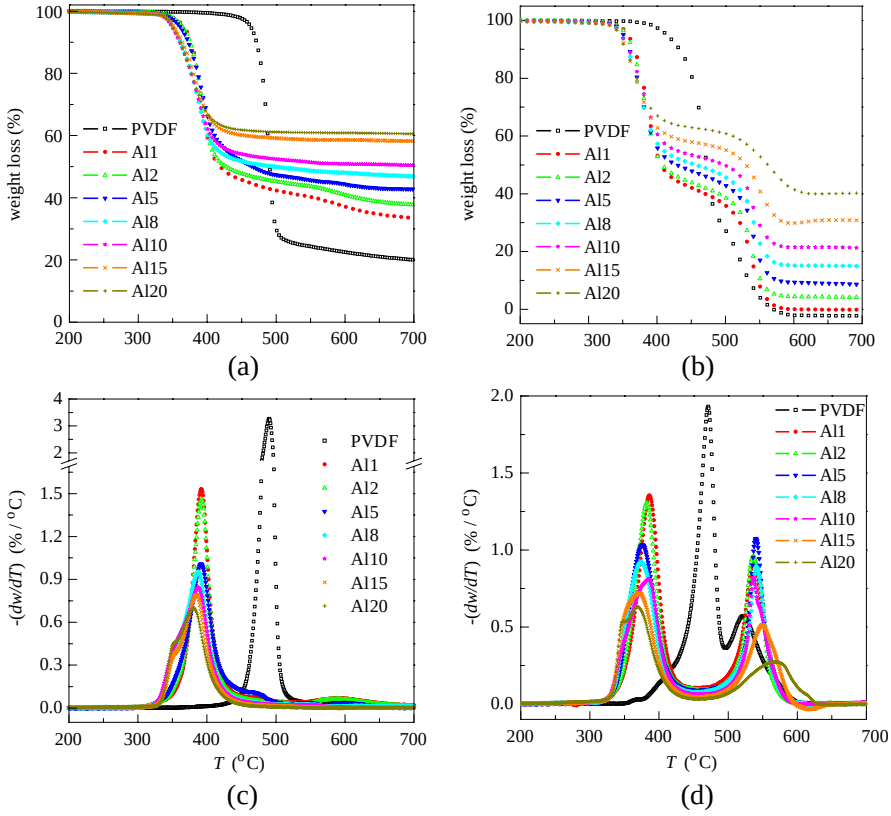

Figure 9. Left plot: (a) TGA and (c) DTGA curves obtained under an inert atmosphere; Right plot: (b) TGA and (d) DTGA curves obtained under an oxidant atmosphere of neat PVDF and the different hybrids analyzed.

any residual at 800°C and the hybrids exhibit similar amounts than those arising from the incorporated Al nanoparticles. Generation of some oxidized species through oxygen uptake is not a significant event if aluminum is used instead of cooper nanoparticles [20].

4. CONCLUSIONS

Hybrids based on PVDF and different amount of Al nanoparticles have been satisfactorily prepared through melt processing. The aluminum particles with nanometric size are randomly distributed within the polymer matrix, with absence of detectable metallic domains of large

size across the bulk. Nevertheless, PVDF crystallinity is affected by Al presence, melting temperatures increase a little in composites with the lowest Al contents and crystallization is shifted to slightly higher temperatures at high Al nanoparticles concentrations because of their nucleating effect. These structural changes also alter the overall mobility, both within amorphous phase and crystalline regions, as well as the rigidity within the hybrids in the whole temperature interval examined. Then, storage modulus values increase as Al concentration is raised, with a rise of around 70% from PVDF to the Al20 hybrid. On the other hand, PVDF thermal decomposition starts at lower temperatures because of the catalytic action of Al nanoparticles.

Dependence of the dielectric characteristics on Al concentration and frequency shows a slight increase in conductivity and permittivity values in the hybrid materials when compared with the pristine PVDF matrix, this rise being more significant in those containing the highest Al contents. Nevertheless, the insulator-conductor transition is not reached within the Al composition range here analyzed.

Finally, EMI shielding effectiveness from attenuation upon reflection evaluated at frequencies ranging from 7 to 15 GHz has demonstrated a loss of reflectivity with relation to the incident radiation in the nanocomposites compared to the pristine PVDF matrix in the whole frequency range analyzed as well as an improvement in the shielding effectiveness of the hybrids with increasing distance between the nanocomposite films and the metal layer. Sample Al10 shows the best balance in properties including, for example, lightness, mechanical performance and shielding behavior.

ACKNOWLEDGMENT

Financial support of Ministerio de Ciencia e Innovación, MICINN (project MAT2010-19883) is acknowledged. J. Arranz-Andrés is grateful to the CSIC JAE-Doc Program for the financial support.

REFERENCES

1. Valente, Jr., W., M. H. Amaral, and A. Raizer, "EMC management: How to compare electromagnetic environmental measurements and equipment immunity levels," *Progress In Electromagnetics Research Letters*, Vol. 18, 165–177, 2010.
2. Chung, D. D. L., "Materials for electromagnetic interference shielding," *J. Mater. Eng. Perform.*, Vol. 9, 350–354, 2000.
3. Afsar, M. N., J. R. Birch, R. N. Clarke, and G. W. Chantry,

"Measurement of the properties of materials," *Proceedings of the IEEE*, Vol. 74, 183–199, 1986.

4. Knott, E. F., J. F. Shaffer, and M. T. Tuley, *Radar Cross Section*, Artech House, 2004.
5. Wu, G., X. Huang, Z. Dou, S. Chen, and L. Jiang, "Electromagnetic interfering shielding of aluminum alloy-cenospheres composite," *Journal of Materials Science*, Vol. 42, 2633–2636, 2007.
6. Wu, G., X. G. Zhang, Z. Q. Song, and B. Liu, "Analysis on shielding performance of metallic rectangular cascaded enclosure with apertures," *Progress In Electromagnetics Research Letters*, Vol. 20, 185–195, 2011.
7. Lei, J. Z., C. H. Liang, and Y. Zhang, "Study on shielding effectiveness of metallic cavities with apertures by combining parallel FDTD method with windowing technique," *Progress In Electromagnetics Research*, Vol. 74, 85–112, 2007.
8. Gorriti, A. G., P. Marin, D. Cortina, and A. Hernando, "Microwave attenuation with composite of copper microwires," *Journal of Magnetism and Magnetic Materials*, Vol. 322, 1505–1510, 2010.
9. Marín, P., D. Cortina, and A. Hernando, "Electromagnetic wave absorbing material based on magnetic microwires," *IEEE Transactions on Magnetics*, Vol. 44, 3934–3937, 2008.
10. Marín, P., D. Cortina, and A. Hernando, "High-frequency behavior of amorphous microwires and its applications," *Journal of Magnetism and Magnetic Materials*, Vols. 290–291, Part 2, 1597–1600, 2005.
11. Wang, Y. and X. Jing, "Intrinsically conducting polymers for electromagnetic interference shielding," *Polymers for Advanced Technologies*, Vol. 16, 344–351, 2005.
12. Das, N. C., T. K. Chaki, D. Khastgir, and A. Chakraborty, "Electromagnetic interference shielding effectiveness of ethylene vinyl acetate based conductive composites containing carbon fillers," *Journal of Applied Polymer Science*, Vol. 80, 1601–1608, 2001.
13. Morari, C., I. Balan, J. Pintea, E. Chitanu, and I. Iordache, "Electrical conductivity and electromagnetic shielding effectiveness of silicone rubber filled with ferrite and graphite powders," *Progress In Electromagnetics Research M*, Vol. 21, 93–104, 2011.
14. Koledintseva, M. Y., J. Drewniak, R. DuBroff, K. Rozanov, and B. Archambeault, "Modeling of shielding composite materials and structures for microwave frequencies," *Progress In Electromagnet-*

ics Research B, Vol. 15, 197–215, 2009.

15. Raj, C. D., G. S. Rao, P. V. Y. Jayasree, B. Srinu, and P. Lakshman, "Estimation of reflectivity and shielding effectiveness of three layered laminate electromagnetic shield at X-band," *Progress In Electromagnetics Research B*, Vol. 20, 205–223, 2010.
16. Jayasree, P. V. Y., V. S. S. N. Srinivasa Baba, B. Prabhakara Rao, and P. Lakshman, "Analysis of shielding effectiveness of single, double and laminated shields for oblique incidence of EM waves," *Progress In Electromagnetics Research B*, Vol. 22, 187–202, 2010.
17. Danaei, M. M., H. Aliakbarian, M. Azarbadegan, and Y. Bairami, "Protection of car-size sensitive equipments using a shielding cover," *Progress In Electromagnetics Research M*, Vol. 7, 97–108, 2009.
18. Qureshi, A., A. Mergen, M. S. Eroglu, N. L. Singh, and A. Gulluoglu, "Dielectric properties of polymer composites filled with different metals," *Journal of Macromolecular Science, Part A: Pure and Applied Chemistry*, Vol. 45, 462–469, 2008.
19. Teirikangas, M., J. Juuti, and H. Jantunen, "Organic-inorganic RF composites with enhanced permittivity by nanoparticle additions," *Progress In Electromagnetics Research*, Vol. 115, 147–157, 2011.
20. Arranz-Andrés, J., E. Pérez, and M. L. Cerrada, "Hybrids based on poly (vinylidene fluoride) and Cu nanoparticles: Characterization and EMI shielding," *European Polymer Journal*, Vol. 48, 1160–1168, 2012.
21. Nalva, H. S., *Ferroelectric Polymers,* Marcel Dekker Inc., New York, 1955.
22. Nagai, M., K. Nakamura, H. Uehara, T. Kanamoto, Y. Takahashi, and T. Furukawa, "Enhanced electrical properties of highly oriented poly (vinylidene fluoride) films prepared by solid-state coextrusion," *Journal of Polymer Science — Part B: Polymer Physics*, Vol. 37, 2549–2556, 1999.
23. Strashilov, V. L., "Efficiency of poly (vinylidene fluoride) thin films for excitation of surface acoustic waves," *Journal of Applied Physics*, Vol. 88, 3582–3586, 2000.
24. Kepler, R. G. and R. A. Anderson, "Ferroelectric polymers," *Advances in Physics*, Vol. 41, 1–57, 1992.
25. Kepler, R. G., *Ferroelectric Polymers: Chemistry, Physics and Applications,* Marcel Dekker, New York, 1995.
26. Tashiro, K., *Ferroelectric Polymers: Chemistry, Physics and*

Applications, Marcel Dekker, New York, 1995.

27. Matsushige, K., "Pressure effect on phase transition in ferroelectic polymers," *Phase Transitions*, Vol. 18, 247–262, 1989.
28. Scheinbeim, J., C. Nakafuku, B. A. Newman, and K. D. Pae, "High-pressure crystallization of poly (vinylidene fluoride)," *Journal of Applied Physics*, Vol. 50, 4399–4405, 1979.
29. Wang, X. C. and Z. Liu, "A new computation of shielding effectiveness of electromagnetic radiation shielding fabric," *Progress In Electromagnetics Research Letters*, Vol. 33, 177–186, 2012.
30. Lucyszyn, S. and Y. Zhou, "Characterising room temperature THz metal shielding using the engineering approach," *Progress In Electromagnetics Research*, Vol. 103, 17–31, 2010.
31. McCrum, N. G., B. E. Read, and G. Williams, *Anelastic and Dielectric Effects in Polymeric Solids*, Dover, New York, 1991.
32. Nakagawa, K. and Y. Ishida, "Annealing effects in poly (vinylidene fluoride) as revealed by specific volume measurements, differential scanning calorimetry, and electron microscopy," *Journal of Polymer Science — Part B: Polymer Physics*, Vol. 11, 2153–2171, 1973.
33. Lovinger, A. J., *Developments in Crystalline Polymers-I*, Applied Science Publishers, London, 1982.
34. Xu, J. and C. P. Wong, "Low-loss percolative dielectric composite," *Applied Physics Letters*, Vol. 87, 2005.
35. Chanmal, C. V. and J. P. Jog, "Dielectric relaxations in PVDF/$BaTiO_3$ nanocomposites," *Express Polymer Letters*, Vol. 2, 294–301, 2008.
36. Linares, A., A. Nogales, D. R. Rueda, and T. A. Ezquerra, "Molecular dynamics in PVDF/PVA blends as revealed by dielectric loss spectroscopy," *Journal of Polymer Science — Part B: Polymer Physics*, Vol. 45, 1653–1661, 2007.
37. Takahashi, Y. and K. Miyaji, "Long-range order parameters of form II of poly (vinylidene fluoride) and molecular motion in the $\hat{I} \pm c$ relaxation," *Macromolecules*, Vol. 16, 1789–1792, 1983.
38. Boyd, R. H., "Relaxation processes in crystalline polymers: Experimental behaviour — A review," *Polymer*, Vol. 26, 323–347, 1985.
39. Boyd, R. H., "Relaxation processes in crystalline polymers: Molecular interpretation — A review," *Polymer*, Vol. 26, 1123–1133, 1985.
40. Tian, L. Y., X. B. Huang, and X. Z. Tang, "Study on

morphology behavior of PVDF-based electrolytes," *Journal of Applied Polymer Science*, Vol. 92, 3839–3842, 2004.

41. Kochervinskii, V. V., I. A. Malyshkina, G. V. Markin, N. D. Gavrilova, and N. P. Bessonova, "Dielectric relaxation in vinylidene fluoride-hexafluoropropylene copolymers," *Journal of Applied Polymer Science*, Vol. 105, 1101–1117, 2007.
42. Panwar, V., J. O. Park, S. H. Park, S. Kumar, and R. M. Mehra, "Electrical, dielectric, and electromagnetic shielding properties of polypropylene-graphite composites," *Journal of Applied Polymer Science*, Vol. 115, 1306–1314, 2010.
43. Yano, S., "Dielectric relaxation and molecular motion in poly (vinylidene fluoride)," *Journal of Polymer Science — Part A-2: Polym. Chem.*, Vol. 8, 1057–1072, 1970.
44. Lovinger, A. J. and T. T. Wang, "Investigation of the properties of directionally solidified poly (vinylidene fluoride)," *Polymer*, Vol. 20, 725–732, 1979.
45. O'Shea, M. L., C. Morterra, and M. J. D. Low, "Spectroscopic studies of carbons. XVII. Pyrolysis of polyvinylidene fluoride," *Materials Chemistry and Physics*, Vol. 26, 193–209, 1990.
46. Zulfiqar, S., M. Zulfiqar, M. Rizvi, A. Munir, and I. C. McNeill, "Study of the thermal degradation of polychlorotrifluoroethylene, poly (vinylidene fluoride) and copolymers of chlorotrifluoroethylene and vinylidene fluoride," *Polymer Degradation and Stability*, Vol. 43, 423–430, 1994.
47. Botelho, G., S. Lanceros-Mendez, A. M. Goncalves, V. Sencadas, and J. G. Rocha, "Relationship between processing conditions, defects and thermal degradation of poly (vinylidene fluoride) in the β-phase," *Journal of Non-Crystalline Solids*, Vol. 354, 72–78, 2008.
48. Kang, D. J., K. Pal, D. S. Bang, and J. K. Kim, "Synergistic effect on crystalline structure of polyvinylidene fluoride nanocomposites with multiwalled carbon nanotube loading by a twin screw extruder," *Journal of Applied Polymer Science*, Vol. 121, 226–233, 2011.